

Photoacoustic measurements of the vibrational relaxation of the selectively excited ozone (ν_3) molecule in pure ozone and its binary mixtures with O₂, N₂, and noble gases

V. Zeninari

Groupe de Spectrométrie Moléculaire et Atmosphérique, UPRES A CNRS 6089, Faculté des Sciences, B.P. 1039 F-51687, REIMS Cedex 2, France

B. A. Tikhomirov and Yu. N. Ponomarev

Laboratory of Atmospheric Spectroscopy, Institute of Atmospheric Optics, Siberian Branch, Russian Academy of Sciences, Tomsk 634055, Russia

D. Courtois

Groupe de Spectrométrie Moléculaire et Atmosphérique, UPRES A CNRS 6089, Faculté des Sciences, B.P. 1039 F-51687, REIMS Cedex 2, France

(Received 19 July 1999; accepted 26 October 1999)

The vibrational-translational relaxation time of the ν_3 state of ozone was deduced from the phase shift of the photoacoustic detector signal relative to the amplitude-modulated radiation of the CO₂ laser used for excitation of O₃. A special photoacoustic cell with a third electrode is used to eliminate an instrumentation phase shift caused by inertia of the microphone membrane. A three-level kinetic model of O₃ is presented and used to fit the experimental and calculated phase shifts to determine the vibrational relaxation rate coefficients for pure O₃ and binary mixtures of O₃ with O₂, N₂, and noble gases He, Ne, Ar, Kr, and Xe. These results are presented and compared with experimental data obtained for O₃, O₃-O₂, and O₃-N₂ by fluorescence and double resonance techniques. Experimental data for ν_3 state relaxation in binary mixtures with all noble atoms have been obtained for the first time. These new results are compared with the simplest model of interaction. Thus we obtain a very good agreement for the decrease of constants with the increase of the colliding partner mass. © 2000 American Institute of Physics. [S0021-9606(00)00904-1]

I. INTRODUCTION

Ozone is one of the most important minor constituents of the terrestrial atmosphere. The knowledge of ozone vibrational relaxation rates, especially in collisions with O₂ and N₂, is of interest for describing the ozone kinetics in the atmosphere and for modeling atmospheric radiative processes.¹

The interpretation of laboratory studies of ozone formation and destruction mechanisms in the mesosphere and thermosphere also depends on the availability of quantitative data on spectroscopic and kinetic parameters.² The main feature of ozone chemistry in the upper atmosphere is that the reactants and products of reactions are not in thermodynamic equilibrium. There exists instead steady-state distribution of molecular energy states, which depend on local temperatures and species concentrations. Modeling such distributions requires a detailed knowledge of reactant—and product-state—specific rate coefficients.³

Moreover the analysis of the chemical reactions in gas mixtures with O₃ being in excited vibrational states needs the same informations. Experimental data on the vibrational relaxation rates for collisions of selectively excited ozone molecules with noble atoms from He to Xe are of interest to check the theory of collisional relaxation of the multilevel quantum systems due to simplicity of the intermolecular potential when the perturber is a neutral and structureless particle.⁴

Most of the experimental data on the kinetic rate constants have been reported for ozone molecules in Refs. 5–11. In these measurements O₃ molecules were excited into the ν_3 state by a pulsed CO₂ laser, and the evolution of the population of this state was monitored by detecting the fluorescence issued from this state,^{5,6} or by probing the absorption with another CO₂ laser,^{7,8} or with a diode laser^{9–11} by use of the IR-IR double resonance method.

The photoacoustic (PA) techniques¹² allow to measure the global time for transformation of the vibrational energy of excited molecules into translational one on all possible channels of relaxation (V-V, V-V', and V-T energy exchange).

The contribution from individual channels and corresponding rates of vibrational relaxation for a certain state can also be determined by PA techniques with the application of the appropriate model of the vibrational structure of the molecule under study.^{13–15}

In the present work we have studied the relaxation of the 001 state of the O₃ molecule by the PA phase shift method. The preliminary testing of this method was reported in Refs. 16 and 17. We have summarized here the results for the selectively excited 001 state relaxation of O₃ for pure O₃ and binary mixtures of O₃-O₂, O₃-N₂, and O₃-noble atoms. These results have been obtained with a three-level kinetic model and compared with experimental data obtained for O₃, O₃-O₂, O₃-N₂, by fluorescence and double resonance tech-

TABLE I. Rate constants for energy transfer between 100 and 001 states of O₃.

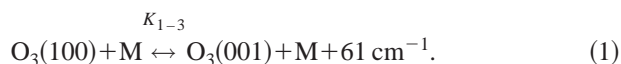
	M=O ₃	M=O ₂	M=N ₂	M=Ar	Ref.
$K_{1-3}(10^6 \text{ s}^{-1} \text{ Torr}^{-1})$	2.18±0.11	0.32±0.08	0.36±0.08	0.32±0.08	7

niques. The series of experimental data for ν_3 state relaxation in binary mixtures with all noble atoms are reported in full version for the first time.

II. KINETIC MODEL OF O₃ VIBRATIONAL LEVELS AND PHASE SHIFT OF PA SIGNAL CALCULATION

¹⁶O₃ is a planar asymmetric rotor belonging to the C_{2v} point group. It has three fundamental vibrations located at $\nu_2 \cong 701 \text{ cm}^{-1}$ (bending), $\nu_3 \cong 1042 \text{ cm}^{-1}$ (asymmetric stretching), and $\nu_1 \cong 1103 \text{ cm}^{-1}$ (symmetric stretching). The rotational levels belonging to the two stretching excited states (100) and (001) are strongly coupled by a Coriolis interaction.

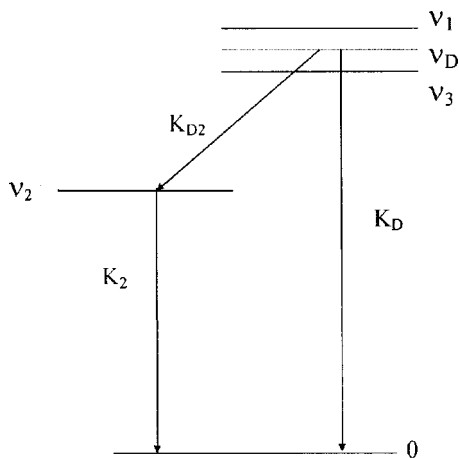
It was shown earlier⁷ that subsequent to exciting the (001) level by a CO₂ laser radiation, a fast equilibrium of the population in this state with that of the (100) state population occurs via the intermode transfer process:



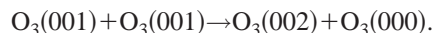
The strong Coriolis interaction coupling of these two levels is certainly responsible for the particularly high efficiency observed for this transfer, specially for pure O₃, (see Table I) in which K_{1-3} is three orders of magnitude greater than the kinetic constants measured in this work.

Taking into account these data we can substitute those two levels with an equivalent one which is denoted *D* and corresponds to (100,001) (Fig. 1).

Figure 1 illustrates the kinetic model used for calculation of the phase shift of the PA signal. The theoretical model is limited to three levels: Dyad (100,001), $\nu_2(010)$, and ground state (000). Such a model has been efficiently used for CO₂ and CH₄.¹⁸ We neglect the interaction of these three levels with higher vibrational levels. This is mainly due to very low

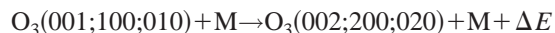
FIG. 1. Three-level kinetic model of O₃(ν_3) deexcitation.

populations of these states at the thermal equilibrium at room temperature. Another reason is that the energy exchange among states 100, 001, 010 and the higher states needs exchange of vibrational energy in collisions of O₃ molecules in excited states, like:



The percentage of O₃ excited molecules is much less than that of unexcited ones (even for pure O₃), so the contribution of this type of collisions is obviously small in binary mixtures of O₃ with buffer gases when $n(\text{O}_3) \ll n(\text{buffer gas})$.

The contribution of the processes like



in the relaxation process seems to also be unlikely.⁴

The influence of the vibrational energy exchange in O₃-O₂ and O₃-N₂ also must be small. The energy differences of the vibrational levels:

$$\Delta E_1 = E_{\text{O}_3(001,100)} - E_{\text{O}_2(\nu=1)} = -484 \text{ cm}^{-1},$$

$$\Delta E_2 = E_{\text{O}_3(001,100)} - E_{\text{N}_2(\nu=1)} = -1258 \text{ cm}^{-1},$$

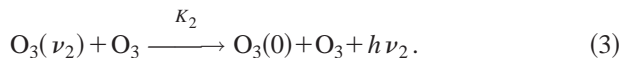
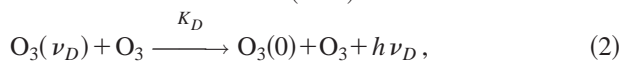
$$\Delta E_3 = E_{\text{O}_3(001)} - E_{\text{O}_2(\nu=1)} = -855 \text{ cm}^{-1},$$

$$\Delta E_4 = E_{\text{O}_3(010)} - E_{\text{N}_2(\nu=1)} = -1629 \text{ cm}^{-1}$$

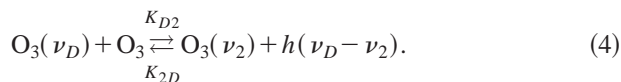
are significantly higher than the necessary value for the efficient intermolecular V.V. exchange.⁴

Collisional energy exchanges taken into account in the three-level model are of two types:

(1) Vibrational-Translational (V.T.):



(2) Vibrational-Vibrational (V.V.):



Exchanges (2), (3), and (4) for the populations n_D ($=n_1+n_3$) of ν_D and n_2 of ν_2 result in the evolution equations:

$$\left(\frac{\partial n_D}{\partial t}\right) = n \cdot K_D(n_D^0 - n_D) + n \cdot K_{D2}(n_D^0 - n_D) - n \cdot K_{2D}(n_2^0 - n_2), \quad (5)$$

$$\left(\frac{\partial n_2}{\partial t}\right) = n \cdot K_2(n_2^0 - n_2) + n \cdot K_{2D}(n_2^0 - n_2) - n \cdot K_{D2}(n_D^0 - n_D). \quad (6)$$

The exponent ‘‘0’’ refers to the populations and the energies in equilibrium and is characterized by the temperature T , n represents the total population, and $K_{D2}/K_{2D} = n_2^0/n_D^0$.

The evolution of the energies of the two vibrational levels is:

$$\left(\frac{\partial e_D}{\partial t}\right) = \zeta_D(e_D^0 - e_D) - \sigma_{D2}(e_2^0 - e_2), \quad (7)$$

$$\left(\frac{\partial e_2}{\partial t}\right) = \zeta_2(e_2^0 - e_2) - \sigma_{2D}(e_D^0 - e_D), \quad (8)$$

where

$$\zeta_D = n(K_D + K_{D2}), \quad (9)$$

$$\sigma_{D2} = n \frac{C_D}{C_2} \left(\frac{v_2}{v_D}\right) K_{D2}, \quad (10)$$

$$\zeta_2 = n \left(K_2 + \frac{C_D}{C_2} \left(\frac{v_2}{v_D}\right)^2 K_{D2} \right), \quad (11)$$

$$\sigma_{2D} = n \left(\frac{v_2}{v_D}\right) K_{D2}, \quad (12)$$

and the heat capacity $C_V = C_{V0} + C_D + C_2$, where C_{V0} corresponds to the translational-rotational part, $C_D (= C_1 + C_3)$ corresponds to the vibrational part of ν_D and C_2 to that of ν_2 .

If we suppose that the periodic laser excitation is described by the fundamental term $\phi = A \exp(j\omega t)$ and that the dynamic pressure P in the cell is $P = \Pi \exp(j\omega t + (\pi/2) - \varphi_1)$. Equation (7) and Equation (8) with conservation of energy in the cell lead to φ_1 :

$$\tan \varphi_1 = \omega \left\{ \frac{(\zeta_D \zeta_2 - \sigma_{D2} \sigma_{2D}) \left[\frac{C_{V0}}{C_V} (\zeta_D + \zeta_2) + \frac{C_2}{C_V} (\zeta_2 - \sigma_{D2}) + \left(\frac{C_D}{C_V} - 1\right) (\zeta_D - \sigma_{2D}) \right] + \omega^2 \frac{C_{V0}}{C_V} (\zeta_D - \sigma_{2D})}{(\zeta_D \zeta_2 - \sigma_{D2} \sigma_{2D})^2 + \omega^2 \left[(\zeta_D - \sigma_{2D}) \left[\frac{C_{V0}}{C_V} (\zeta_D + \zeta_2) + \frac{C_2}{C_V} (\zeta_2 - \sigma_{2D}) + \frac{C_D}{C_V} (\zeta_D - \sigma_{2D}) \right] - \frac{C_{V0}}{C_V} (\zeta_D \zeta_2 - \sigma_{D2} \sigma_{2D}) \right]} \right\}.$$

To this value of φ_1 we must add heat relaxation of the gas in the cell:¹⁹

$$\varphi_2 = \arctan(\omega \tau_T P),$$

where τ_T is the heat relaxation time is defined as:

$$\frac{1}{\tau_T} = \frac{1}{\tau_{TR}} + \frac{1}{\tau_{TC}},$$

with thermal relaxation time $\tau_{TR} = \tau_{TR}^0 / P$ and

$$\tau_{TR}^0 = \frac{\rho C_V D^2}{10\lambda} \text{ at } P_0 = 1 \text{ Torr.}$$

Here ρ (kg m^{-3}) is the gas density, D (m) is the PA cell diameter, C_V ($\text{J kg}^{-1} \text{K}^{-1}$), and λ ($\text{W m}^{-1} \text{K}^{-1}$) are the thermal capacity and thermal conductivity of the gas under study.

The parameter τ_{TC} is the relaxation of the pressure via the capillary of the microphone and equals to $5 \times 10^{-4} \text{ s Torr}^{-1}$ for our PA cell. For pure ozone we estimate $\tau_{TR} = 10^{-3} \text{ s Torr}^{-1}$. The total theoretical value of the phase shift of PA signal oscillations relative to the oscillations of a pumped radiation intensity is determined as

$$\varphi = \varphi_1 + \varphi_2.$$

Figures 2 and 3 give the plots of the values of φ_1 and φ_2 calculated for several values of the modulation frequency ω . These figures show that the choice of a frequency around 2000 Hz is the best compromise to obtain valuable information on the parameters.

III. INSTRUMENTATION

The diagram of the experimental setup is sketched in Fig. 4.

The ozone molecules of the tested gas mixture inside the PA cell are periodically excited to the ν_3 state by the radiation of a cw CO_2 laser modulated by a mechanical chopper at frequency f . The modulation of the gas pressure due to the absorption of the laser radiation is measured at the same frequency by the high-sensitive capacitance microphone of the PA cell.

The electric signal from the microphone is sent to a lock-in amplifier used as a phasemeter to measure the phase shift of the periodic PA signal.

The laser (Model SAT C7-France) is a continuous wave $^{12}\text{C}^{18}\text{O}_2$ isotope waveguide laser. The wave number used for pure ozone studies is $\nu = 1064.1348 \text{ cm}^{-1}$ (9P26 line). The closest ozone line is the line (52, 11, 42 ← 51, 11, 41) of the ν_3 band. Its wave number is $1064.1401 \text{ cm}^{-1}$ and its intensity is $1.22 \times 10^{-22} \text{ cm}^{-1}/(\text{molecule cm}^{-2})$.²⁰ We chose this

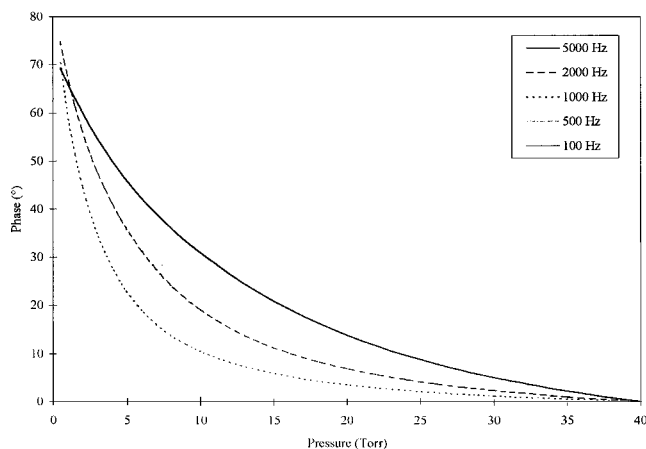
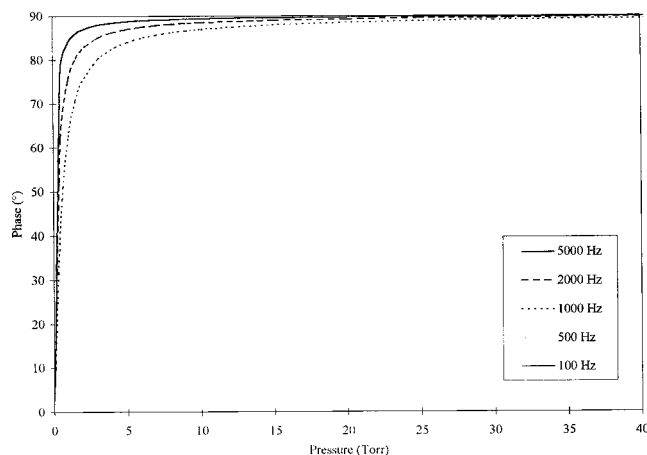


FIG. 2. φ_1 at different modulation frequencies.

FIG. 3. φ_2 at different modulation frequencies.

rather weak line to neglect the attenuation of the laser beam inside the PA cell. We check that even if we have the maximum ozone pressure (40 Torr) the PA cell transmission is still more than 90%.

The laser radiation modulation is obtained by a high-precision mechanical chopper (EG&G model 197). The modulation frequency ($f = \omega/2\pi$) was 1800 Hz, 1900 Hz, or 2000 Hz.

The stainless steel PA cell with BaF₂ windows has 15 mm diameter and 100 mm length.

The design of the laboratory-made microphone is illustrated by Fig. 5.

The initial capacitance of the microphone is 76 pF. The nickel membrane has a 4 μm thickness. The permanent polarization voltage is 120 V and can be varied from 20 to 120 V. A technical peculiarity of the microphone is an additional electrode called an electrode-activator. This electrode is typically used for the calibration of the microphone or for determination of its sensitivity.²¹

In the present work it is used to determine the apparatus phase shift φ_3 caused by the microphone membrane inertia.

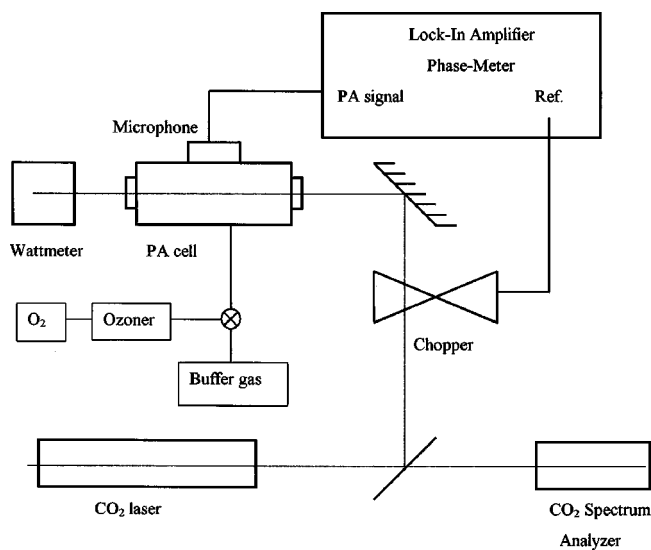


FIG. 4. Schematic diagram of the photoacoustic spectrometer.

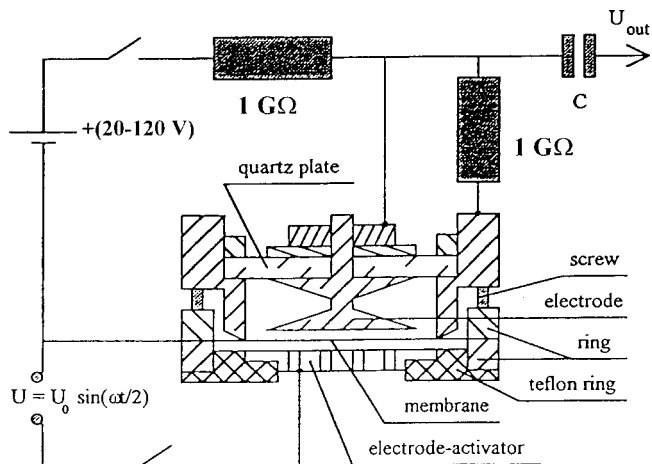


FIG. 5. Schematic diagram of the laboratory-made microphone with electrode-activator.

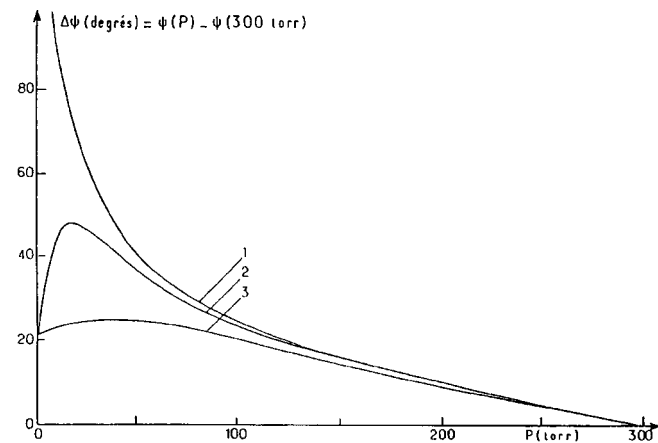
A periodic force of the gas pressure on the membrane is simulated by the periodic force of electrostatic attraction between the membrane and electrode-activator.

A lock-in amplifier (Model M5301 EG&G Princeton Applied Research) with quality factor $Q = 20$ and integration time $\tau = 1$ s is used as a phasemeter. The phase shifts have been measured with an accuracy of ± 0.1 degree.

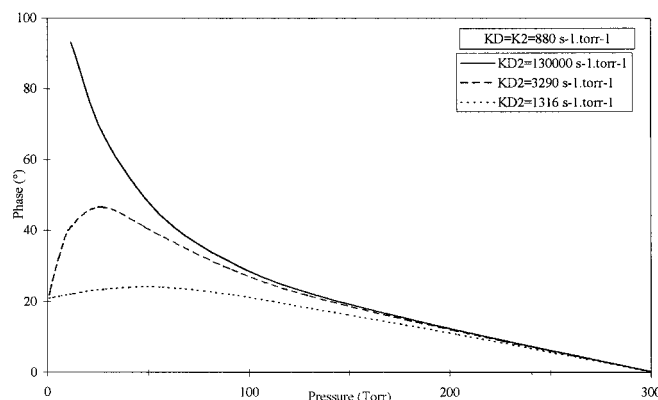
The ozone is prepared by total conversion of ultra pure oxygen. The design of the ozoner was similar to that of Griggs.²² It consists of a cylinder pyrex capacitor. The electrodes are made of copper foil in close contact with the glass, and the applied voltage is 12 kV/400 Hz. High purity oxygen (N45) supplied by Air Liquide-France has the following characteristics: H₂O ≤ 5 ppmv, CO₂ ≤ 0.5 ppmv, N₂ ≤ 10 ppmv, CO ≤ 0.5 ppmv, CH₄ ≤ 0.5 ppmv, and Ar ≤ 10 ppmv. Sixty Torr of gaseous oxygen is introduced into the ozoner. This capacitor is immersed into a dewar containing liquid nitrogen. At this temperature the vapor pressure is 130 Torr for oxygen and 2×10^{-3} Torr for ozone, so oxygen is converted to ozone in the discharge and condensed. The conversion is completed when a purple glow can be seen inside the discharge capacitor. At this point we pump on the liquid ozone to remove the residual oxygen. Then the ozoner is warmed at room temperature and ozone is vaporized into the cell (up to $P \approx 40$ Torr).

Our system—photoacoustic cell, microphone, tubes, and valves—is made of stainless steel. Only teflon or stainless steel rings are used, so our experimental arrangement is ozone proof. The ozone pressure is measured by an MKS baratron model 122AA capacitance manometer. We have estimated the ozone pressure stability to be about 0.2% during the experiment. The method to measure the absolute amount of ozone has been carefully checked with low pressures in absolute intensities measurements.²³ In the case of higher pressures (20–40 Torr), the uncertainty of O₃ concentration measurements is lower than 2%.

The other gases used as perturbers were also of high purity (Air Liquide, France): O₂ (H₂O < 2 ppmv, CO < 0.2 ppmv, CO₂ < 0.2 ppmv); N₂ (H₂O < 3 ppmv, O₂ < 3 ppmv, CO < 1 ppmv); He (H₂O < 2 ppmv, CO < 0.2



(a)



(b)

FIG. 6. (a) Sensitivity on K_{42} of the model calculated by Lepoutre. (b) Sensitivity on K_{42} of the model calculated by us.

ppmv, $\text{CO}_2 < 0.2$ ppmv, $\text{N}_2 < 1$ ppmv, $\text{O}_2 < 0.5$ ppmv, $\text{Ne} < 0.5$ ppmv); Ne ($\text{H}_2\text{O} < 1$ ppmv, $\text{N}_2 < 5$ ppmv, $\text{He} < 4$ ppmv, $\text{O}_2 < 1$ ppmv, $\text{CH}_4 < 0.5$ ppmv); Ar ($\text{H}_2\text{O} < 3$ ppmv, $\text{N}_2 < 10$ ppmv, $\text{O}_2 < 3$ ppmv); Kr ($\text{H}_2\text{O} < 4$ ppmv, $\text{N}_2 < 20$ ppmv, $\text{O}_2 < 4$ ppmv, $\text{Ar} < 10$ ppmv, $\text{Xe} < 10$ ppmv, $\text{H}_2 < 1$ ppmv); and Xe ($\text{H}_2\text{O} < 3$ ppmv, $\text{N}_2 < 20$ ppmv, $\text{O}_2 < 3$ ppmv, $\text{Kr} < 50$ ppmv, $\text{Ar} < 5$ ppmv, $\text{H}_2 < 2$ ppmv).

For pure ozone experiment the ozone pressure is very well known. In the case of mixtures they have been prepared

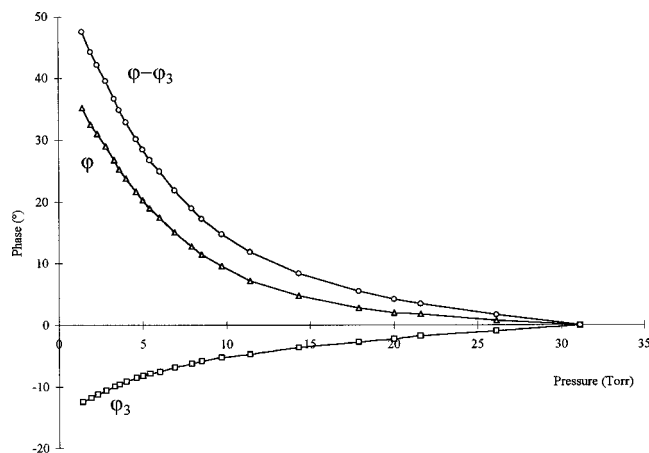


FIG. 7. Example of phase correction vs pressure of pure O_3 .

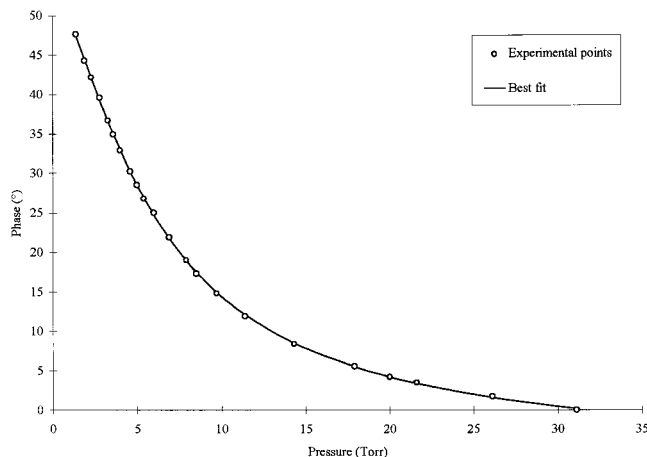


FIG. 8. Result of a fit with the three-level model for pure O_3 .

directly in the cell by adding the buffer gas slowly. These conditions may induce small shock decomposition of ozone in the cell. But this is not critical since the exact knowledge of the concentration is not needed in the fitting program. The main point is that the partial pressure of ozone is lower than 1% and that there is enough signal to make the phase measurement.

For each total pressure we have measured the values of the total phase shift $\varphi = \varphi_1 + \varphi_2 + \varphi_3$ and the correction φ_3 . The correction of the microphone inertia φ_3 is necessary to avoid errors in the determination of the kinetic constants.

IV. FITTING PROCEDURE: DESCRIPTION AND TESTING

The kinetic model described in the previous part is introduced in a least-square fitting procedure. We entered the corrected phase ψ vs P (pressure). The experimental values of $\psi = \varphi_{\text{measured}} - \varphi_3 = (\varphi_1 + \varphi_2)_{\text{measured}}$ vs P (pressure) are compared with the corresponding calculated curve $\psi_{\text{calc.}}(P) = \varphi_{1\text{calc.}}(P) + \varphi_{2\text{calc.}}(P)$, and the rate constants K_{D2} , K_D , and K_2 are determined from the fitting.

At first our model and program have been checked with the results obtained by Lepoutre¹⁸ for CH_4 . The program has been adapted to O_3 . Figure 6 represents the calculated curves by Lepoutre (a) and ours (b) to verify the sensitivity of the model versus one constant. The curves represented in Fig. 6(a) are calculated at $f = 10^5$ Hz with lifetimes (reciprocal rate constants) $\tau_2 = \tau_4 = 1.5 \mu\text{s atm}$ and $\tau_{42} = 10^{-2} \mu\text{s atm}$ (curve 1), $0.4 \mu\text{s atm}$ (curve 2), and $1 \mu\text{s atm}$ (curve 3).¹⁸ Our calculations with the equivalent constants given in Fig. 6(b) for the same frequency were comparable, and this test demonstrates that there is no error in our calculation program.

Then we test the influence of noise in measurements on uncertainties. We proceed by simulation of the experimental curve from a synthetic curve plus Gaussian noise with different signal-to-noise ratios. In a general way we see that besides the increase of the uncertainty of constants when the signal-to-noise ratio decreases, the fitted values are quite near the real ones. This test leads to the conclusion that for a given signal-to-noise ratio the correct constants can be derived with an acceptable error.

TABLE II. Rate coefficients for V.V. and V.T. transfer of pure O₃.

Authors	K_{D2}	K_D	K_2	K_{D2}/K_2
Rosen and Cool ^a	8600^{+4900}_{-3700}	...	2860^{+500}_{-410}	3.01
Hui, Rosen, and Cool ^b	5600^{+1650}_{-2000}	...	2850^{+850}_{-400}	1.96
Ménard-Bourcin, Doyennette, and Ménard ^c	2800 ± 500	600 ± 400	2250 ± 300	1.24
Ménard-Bourcin, Ménard, and Doyennette ^d	2800 ± 200	340^{+360}_{-220}	2150 ± 90	1.30
This work	4400 ± 600	850 ± 450	2000 ± 350	2.20

^aFluorescence technique: Ref. 5.^bFluorescence technique: Ref. 6.^cIR-IR double-resonance technique: Ref. 7.^dIR-IR double-resonance technique: Ref. 8.

V. RESULTS AND DISCUSSION

A. O₃(001) relaxation in pure ozone

Many series of measurements of φ and φ_3 for pure O₃ by decreasing the total pressure from 35 to 1 Torr have been made. A typical view of the measured plots of φ and φ_3 and their difference $\varphi - \varphi_3$ is shown in Fig. 7. The results of fitting of $(\varphi_1 + \varphi_2)_{\text{calc.}}$ (full line) with $\varphi - \varphi_3$ (points) is shown as an example on Fig. 8. In all cases the residual error is smaller than 0.3°, which is in the order of the accuracy of our phasemeter. The values of the rate constants K_{D2} , K_D , and K_2 and their relative errors have been determined by statistical averaging of the measured values. The application of the three-level model for the ozone molecule gives us a rather good fitting of experimental and calculated plots of the phase shift and the possibility to determine all the rate constants of vibrational relaxation for this model. Our values of rate constants K_{D2} , K_D , and K_2 are summarized and compared with that of different authors in Table II.

We can notice that for K_D and K_2 our results are in good agreement with all other results included in Table II. As for the other methods, the uncertainty in K_D is relatively large because the three-level model is less sensitive to this constant than to the two others. For K_{D2} it seems that our value is closer to the value obtained by fluorescence technique. The ratio K_{D2}/K_2 (i.e., the ratio of the rate constants which

are determined with less uncertainty) obtained in our measurements is centered on the series of earlier measurements.

The results presented in Table II show that de-excitation of the 001 state of O₃ occurs mainly in two steps: $\nu_D \rightarrow \nu_2$ then $\nu_2 \rightarrow 0$ and only a small part of the molecules de-excite themselves by the direct way $\nu_D \rightarrow 0$.

B. O₃(001) relaxation in O₂, N₂

The measurements of O₃(001) relaxation have been done for O₃-M (M=N₂,O₂) mixtures with O₃ relative concentration near 10⁻³ and total pressure decreasing from 700 Torr to 1 Torr. The CO₂ 9P20 laser line centered at 1068.9425 cm⁻¹ was used for O₃(001) pumping. This laser line is near the (49, 6, 43 ← 48, 6, 42) absorption line ($\nu_0 = 1068.9433$ cm⁻¹) with an intensity 0.911×10^{-21} cm⁻¹/(molecule cm⁻²).²⁰ The modulation frequency is $f = 1800$ Hz. The results of the phase fitting $\varphi - \varphi_3$ measured and $\varphi_1 + \varphi_2$ calculated for the both perturbers O₂ and N₂ are presented in Figs. 9 and 10.

Tables III and IV gather the obtained mean values for the kinetic constants, their uncertainties as well as the ratio K_{D2}/K_2 , and are compared with earlier literature data.

For O₃-O₂, O₃-N₂ mixtures (i.e., for O₃-air, also) the deactivation of 001 comes through the 010 state and the direct contribution of 001 to 000 relaxation is practically negligible. Our results for O₃-O₂ are in satisfactory agree-

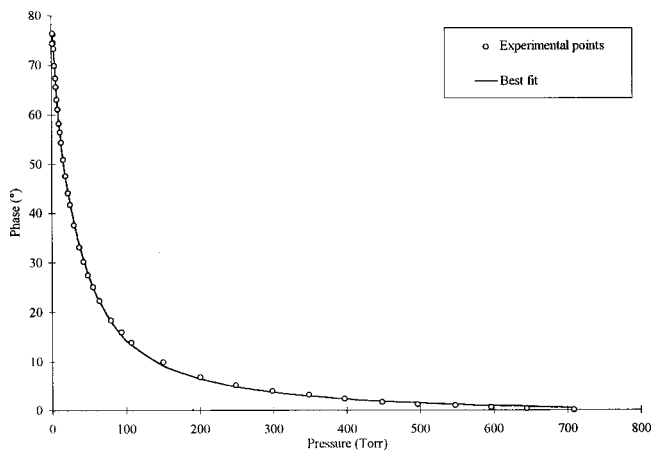
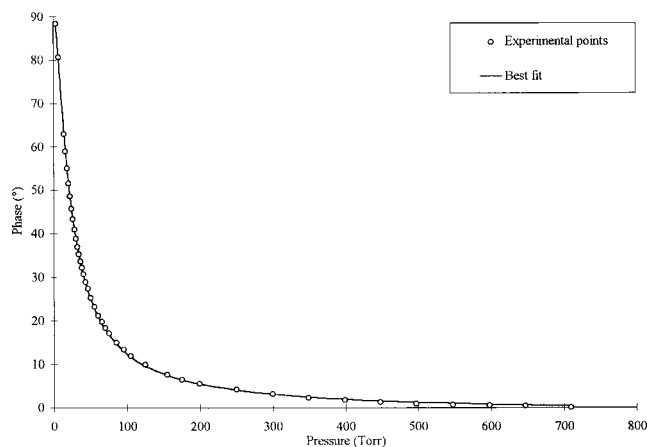
FIG. 9. Result of a fit with the three-level model for the mixture O₃-O₂.FIG. 10. Result of a fit with the three-level model for the mixture O₃-N₂.

TABLE III. Rate coefficients for V.V. and V.T. transfer for O_3-O_2 .

Authors	K_{D2}	K_D	K_2	K_{D2}/K_2
West <i>et al.</i> ^a	1200 ± 600	-	650 ± 200	1.85
Adler-Golden <i>et al.</i> ^b	1670 ± 370	-	990 ± 110	1.69
Joens <i>et al.</i> ^c	310 ± 50	-	750 ± 150	0.41
Ménard-Bourcin <i>et al.</i> ^d	950 ± 90	<100	1100 ± 100	0.86
This work	1350 ± 150	<10	750 ± 100	1.8

^aFluorescence technique: Ref. 24.^bIR-UV double resonance technique: Ref. 25.^cAbsorption technique: Ref. 26.^dIR-IR double resonance technique: Ref. 8.

ment with the data obtained in Refs. 24 and 25 for absolute values of K_{D2} and K_2 . The agreement between the ratio K_{D2}/K_2 for O_3-N_2 in our measurements and in Ref. 8 is also good.

One of the possible explanations of the difference between the results of this work and the others obtained might be the gas purity. In our experiments we have used gas mixtures with gases of different quality (from 99.95% to 99.999%). We have seen that even a very small part of H_2O or C_nH_m may change the rate constants and in our three-model it appears as an artificial increasing of the constant K_2 . That is why our present results are obtained with ultra-grade purity gases (99.999%). Moreover, as we say in the experimental part, in our measurements the influence of small chock decomposition of ozone by introducing the buffer gas has no importance since the absolute ozone amount is not need in the fitting program.

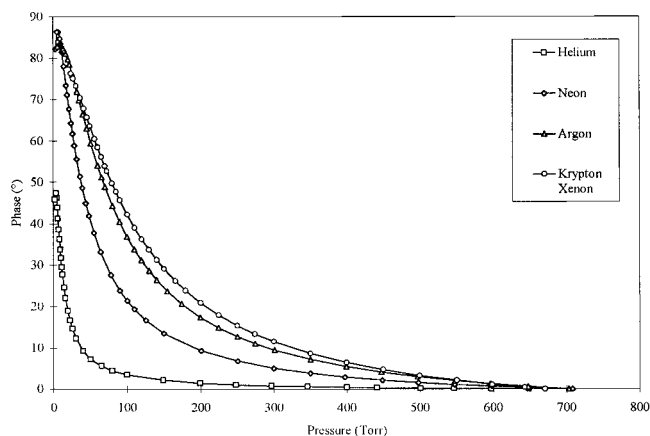
C. $O_3(001)$ relaxation in noble gases

The modulation frequency used to study the $O_3(001)$ relaxation kinetics in mixture with noble gases (Helium, Neon, Argon, Krypton, and Xenon) is 1800 Hz. The CO_2 laser line and O_3 absorption line are the same as in the case of O_3-O_2 and O_3-N_2 mixtures. The pressure of O_3 -noble gas mixture with ozone relative concentration near 10^{-3} and total pressure are decreasing from 700 Torr to 1 Torr. The procedure of the phase shift measurements and determination of K_{D2} , K_D , and K_2 are also the same. Figure 11 presents the fitting of the results for all kinds of noble atoms. The krypton and xenon curves are practically the same. The average values of the rate coefficients and the corresponding uncertainties are summarized in Table V.

We may again conclude that the deactivation of the 001 state of O_3 directly to the 000 state is not effective in comparison with the step deactivation via 010 level. The rate coefficients of K_{D2} and K_2 are monotonically decreasing from He to Xe.

TABLE IV. Rate coefficients for V.V. and V.T. transfer for O_3-N_2 .

Authors	K_{D2}	K_D	K_2	K_{D2}/K_2
Ménard-Bourcin <i>et al.</i> ^a	1300 ± 100	<100	1000 ± 120	1.30
This work	900 ± 100	<10	700 ± 50	1.28

^aIR-IR double resonance technique: Ref. 8.FIG. 11. Result of a fit with the three-level model for the mixtures O_3 -noble gases.

We have plotted also the dependence of the ratio of K_{D2}/K_2 vs polarizability α of the collisional partner noble atom (Fig. 12).

The behavior of the ratio K_{D2}/K_2 is practically identical to the dependence of the ratio of the broadening coefficients of the rotational-vibrational spectral lines of the fundamental bands of some polar molecules like NO_2 and SO_2 , observed in Ref. 27.

Figure 13 illustrates the similarity of the behavior of the ratio $\gamma(XO_2-A)/\gamma(XO_2-Xe)$ and that of the K_{D2}/K_2 for O_3-A , where A means He, Ne, Ar, Kr, and Xe, and X corresponds to N or S.

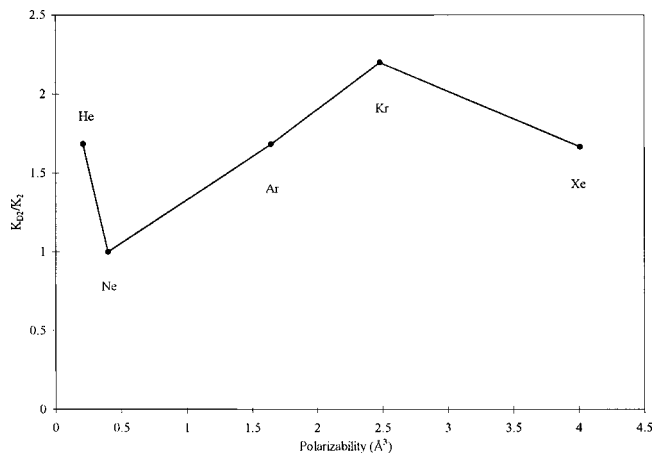
We may explain this similarity by the significant contribution of the short-range forces in polar molecule-noble atom collisions not only to the vibrational energy relaxation,⁴ but also to the collisional line broadening. It would be interesting to obtain the results of O_3 line broadening by noble gas pressure for 001 band and to apply them together with data on vibrational relaxation rate coefficients for determination of parameters of the short-range part of the intermolecular potential for O_3 -noble atom collisions.

In the simplest case of O_3 -noble atom interaction we have estimated the vibrational relaxation rate constants using the Landau-Teller approximation.⁴ According to this approximation the rate constant for transition between neighboring vibrational states is given by the expression:

$$K_{v,v+1} = \sigma \sqrt{\frac{kT}{\mu}} (v+1) C(T, \nu) \times \exp \left[-3 \left(\frac{\omega l_0 \sqrt{M}}{\sqrt{2kT}} \right)^{2/3} \right], \quad (13)$$

TABLE V. Rate coefficient for V.V. and V.T. transfer for O_3 -noble gases.

	K_{D2}	K_D	K_2	K_{D2}/K_2
He	3200 ± 200	460 ± 70	1900 ± 400	1.68
Ne	470 ± 50	<10	470 ± 50	1.00
Ar	320 ± 60	<10	190 ± 10	1.68
Kr	220 ± 20	<10	100 ± 10	2.20
Xe	200 ± 30	<10	120 ± 20	1.67

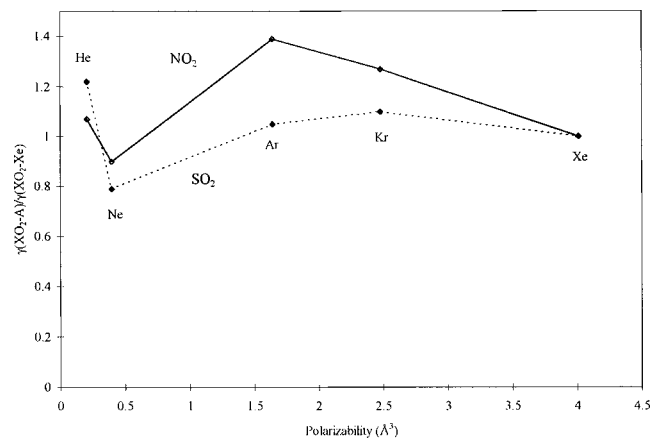
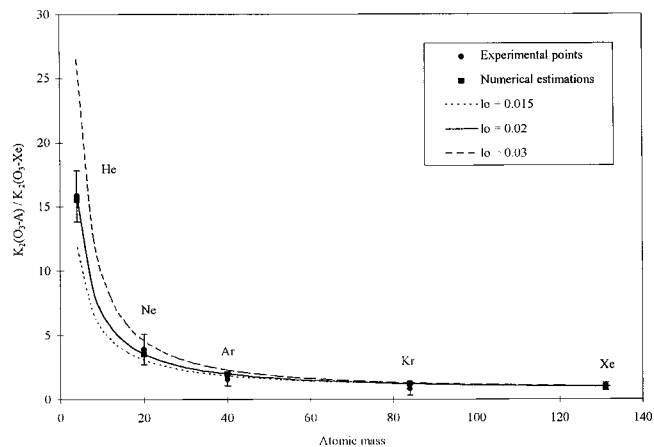
FIG. 12. Ratio K_{D2}/K_2 vs polarizability of the noble atom.

where σ is the collisional cross section, k is the Boltzmann constant, ν is the frequency of the transition, T is the gas temperature, μ is the reduced mass of the colliding particles, l_0 is the scale parameter for the trajectory with impact parameter $b=0$, and $C(T, \nu)$ is a function slowly depending on the temperature.

We have calculated the rate constant K_2 for collisions with He, Ne, Ar, Kr, and Xe when l_0 is varying from 0.01 to 0.04 Å. Figure 14 shows the calculated dependence of the ratio of $K_2(O_3-A)/K_2(O_3-Xe)$ on mass of perturbers for several l_0 . The best agreement of calculated and observed data is for $l_0=0.02$ Å. Also the formula Eq. (13) with $l_0=0.02$ Å reproduces in a rather well way the same dependence for the ratio $K_{D2}(O_3-A)/K_{D2}(O_3-Xe)$ on the atomic mass (Fig. 15).

VI. CONCLUSION

The PA method has been used to estimate the vibrational relaxation rate constants of (001) state of pure O_3 and O_3 mixtures with O_2 , N_2 (main atmospheric components), and the noble gases He, Ne, Ar, Kr, and Xe. This method pre-

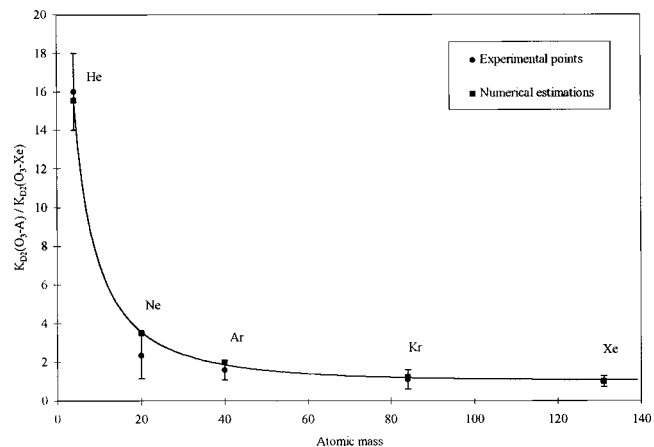
FIG. 13. $\gamma(XO_2-A)/\gamma(XO_2-Xe)$ behavior vs polarizability of the noble atom.FIG. 14. $K_2(O_3-A)/K_2(O_3-Xe)$ vs atomic mass for different values of l_0 .

sents the advantages of comparative simplicity and a wide spectral coverage since the infrared detector is replaced with a microphone whatever the region.

The obtained results in the present work show that the O_3-O_3 collisions are more efficient than the O_3-O_2 and O_3-N_2 collisions to transfer the vibrational energy from (100,001) to (010) and to deexcite (010). All these results are in quite good agreement with previous results for O_3 .

The similar model for the stretching vibrational modes relaxation seems also acceptable to us for the H_2O molecule. In Refs. 28, 29 the obtained experimental data show that the fast transfer of vibrational energy from $n\nu_1 + m\nu_3$ mode to $n\nu_2$ with next relaxation within $n\nu_2$ mode takes place. The confirmation of this conclusion is the fact of $\tau_{VT}(103)$ measured by the PA method²⁷ is less than the corresponding value given for the relaxation of $00n \rightarrow 000$ channel from the fluorescence techniques.

Besides we have for the first time calculated the rate coefficients of O_3 in mixture with the main noble gases. We have shown that the rate coefficients decrease with the increase of the mass of the collision partner for the O_3 -noble atom collisions. These results have been compared with the simplest model of interaction, and we obtain a good agreement for the decreasing of the constants ratio for all perturbers.

FIG. 15. $K_{D2}(O_3-A)/K_{D2}(O_3-Xe)$ vs atomic mass for $l_0=0.02$ Å.

ACKNOWLEDGMENTS

The authors would like to express their gratitude to Engineer Antoine Luna for his helpful contribution to this work. This paper has been prepared with the partial support of the Russian Basic Research Foundation (Project No. 99-05-64564).

- ¹J. A. Joens, J. B. Burkholder, and E. J. Bair, *J. Chem. Phys.* **76**, 5902 (1982).
- ²W. T. Rawlins, G. E. Caledonia, and J. P. Kennealy, *J. Geophys. Res.* **86**, 5247 (1981).
- ³J. I. Steinfeld, S. M. Adler-Golden, and J. W. Gallagher, *J. Phys. Chem. Ref. Data* **16**, 911 (1987).
- ⁴V. N. Kondratiev, E. E. Nikitin, “*Kinetics and Mechanisms of Chemical Reaction in Gases*” (in Russian) (Nauka, Novosibirsk, 1981).
- ⁵D. I. Rosen and T. A. Cool, *J. Chem. Phys.* **62**, 466 (1975).
- ⁶K. K. Hui, D. I. Rosen, and T. A. Cool, *Chem. Phys. Lett.* **32**, 141 (1975).
- ⁷F. Ménard-Bourcin, L. Doyennette, and J. Ménard, *J. Chem. Phys.* **92**, 4212 (1990).
- ⁸F. Ménard-Bourcin, J. Ménard, and L. Doyennette, *J. Chem. Phys.* **94**, 1875 (1991).
- ⁹C. Flannery, Y. Mizugai, J. I. Steinfeld, and M. N. Spencer, *J. Chem. Phys.* **92**, 5164 (1990).
- ¹⁰C. C. Flannery and J. I. Steinfeld, *J. Chem. Phys.* **96**, 8157 (1992).
- ¹¹C. C. Flannery, J. I. Steinfeld, and R. R. Gamache, *J. Chem. Phys.* **99**, 6495 (1993).
- ¹²P. V. Slobodskaya, *Izv. Akad. Nauk SSSR, Ser. Fiz.* **12**, 656 (1948).
- ¹³H. J. Bauer, *J. Chem. Phys.* **57**, 3130 (1972).
- ¹⁴R. Tripodi and W. G. Vincenti, *J. Chem. Phys.* **54**, 2207 (1971).
- ¹⁵J. Taine, F. Lepoutre, and G. Louis, *Chem. Phys. Lett.* **58**, 611 (1978).
- ¹⁶V. Zéninari, B. A. Tikhomirov, Yu. N. Ponomarev, and D. Courtois, *J. Quant. Spectrosc. Radiat. Transf.* **59**, 369 (1998).
- ¹⁷D. Courtois, B. Parvitte, Yu. N. Ponomarev, O. V. Tikhomirova, B. A. Tikhomirov, and V. Zéninari, *Chinese J. Acoustics* **16**, 372 (1997).
- ¹⁸F. Lepoutre, Thesis, Université de Paris-Sud, Center d’Orsay, France, 1979.
- ¹⁹L. B. Kreuzer, *J. Appl. Phys.* **42**, 2934 (1971).
- ²⁰L. S. Rothman, R. R. Gamache, R. H. Tipping, C. P. Rinsland, M. A. H. Smith, D. C. Benner, V. Malathy Devi, J.-M. Flaud, C. Camy-Peyret, A. Perrin, A. Goldman, S. T. Massie, L. R. Brown, and R. A. Toth, *J. Quant. Spectrosc. Radiat. Transf.* **48**, 469 (1992).
- ²¹A. B. Antipov, V. A. Kapitanov, Yu. N. Ponomarev, and V. A. Sapozhnikova, “*Photoacoustic Method in Laser Spectroscopy of Molecular Gases*” (Nauka, Novosibirsk, 1984).
- ²²M. Griggs, *J. Chem. Phys.* **49**, 857 (1968).
- ²³M. R. De Backer-Barilly and D. Courtois, *Appl. Phys. B: Lasers Opt.* **64**, 607 (1997).
- ²⁴G. A. West, R. E. Weston, Jr., and G. W. Flynn, *Chem. Phys. Lett.* **56**, 429 (1978).
- ²⁵S. M. Adler-Golden and J. I. Steinfeld, *Chem. Phys. Lett.* **76**, 479 (1980).
- ²⁶J. A. Joens, J. B. Burkholder, and E. J. Bair, *J. Chem. Phys.* **76**, 5902 (1982).
- ²⁷V. V. Lazarev, Yu. N. Ponomarev, B. Sumpf, O. Fleischmann, J. Waschull, H.-D. Kronfeldt, and V. Stroinova, *J. Mol. Spectrosc.* **173**, 177 (1995).
- ²⁸V. A. Kapitanov, O. Yu. Nikiforova, Yu. N. Ponomarev, and B. A. Tikhomirov, *Atmos. Ocean Opt.* **7**, 1463 (1994).
- ²⁹J. Finzi, F. E. Hovic, V. N. Panfilov, P. Hess, and C. B. Moore, *J. Chem. Phys.* **67**, 4053 (1977).